Experimental investigation of a U-tube thermocell under various $Fe(CN)_6^{3-/4-}$ concentration

Gao Qian [a,b], Xiaoli Yu [a,b], Zhi Li [a,b,*], Jiarong Wu [a,b], Rui Huang [a,b], Yiji Lu [a,c,*]

[a] *Department of Energy Engineering, Zhejiang University, Hangzhou, 310027, China*

[b] *Ningbo Research Institute, Zhejiang University, Ningbo, 315100, China*

[c] *Durham Energy Institute, Durham University, Durham, DH1 3LE, United Kingdom*

HIGHLIGHTS

- Electrolyte with different concentration ratios are studied in a U-tube thermocell
- A rapid temperature control module is designed based on a thermoelectric cooler
- Total concentration and concentration ratio have a significant effect on a thermocell
- Activity coefficient in the solubility calculation can be ignored
- Adjusting concentration is feasible to optimise thermocell performance

Abstract:

Research interest in thermocell technology has been increasingly occurring due to its large Seebeck coefficient (~1 mV/K) and flexible structure, which are its unique advantages for use in wearable devices directly converting thermal energy into electricity. It is timely and critical to investigate the technology to potentially overcome the technological drawbacks of thermocell such as its relatively low power density and limited overall energy efficiency. In this paper, the correlation between the performance of a $Fe(CN)_6^{3-/4-}$ thermocell and ion concentrations are studied through factorial experiments. Solubility tests are conducted to obtain the maximum concentration. Activity coefficient is found non-negligible in the Nernst equation. The saturation line calculated through concentration solubility product shows relatively close agreement with experimental results. Total concentration, as well as the concentration ratio of ions, have a significant effect on the thermocell performance. At the optimised concentration point on the saturation line, power density, Seebeck coefficient and efficiency respectively increase by 7.38%, 8.93% and 5.69%. And the mass of solute decreases by 12.64%, compared with the widely used 1:1 concentration ratio. Results demonstrate to improve the power density of thermocell, the solution needs to be saturated and the ion concentration ratio should be taken into account.

Keywords: Thermocell, Factorial experiment, Concentration, Performance optimisation, Thermal energy conversion

E-mail address: liz_ym@zju.edu.cn *(Z. Li)*
luyiji0620@gmail.com; *(Y. Lu)*

1. Introduction

One of the most critical thermal energy research challenges is the efficient and effective utilisation of low-grade thermal energy (<130 °C), converting thermal energy to useful energies such as cooling, electricity or upgraded heat without generating emissions. Technologies such as thermoelectric generation system [1-3], sorption technologies [4-6] and Organic Rankine cycle [7-9] have been extensively investigated and developed worldwide.

Most recently, emerging technologies based on electrochemistry directly converting thermal energy to electricity [10, 11] received increasing attention. Fig. 1 shows the classification of techniques for direct conversion of low-grade thermal energy to electricity. According to the causes of electromotive force, electrochemical techniques can be classified into the following two types. The first type results by the concentration difference including the reverse electrodialysis (RED) system [12] and the thermally regenerative ammonia-based battery (TRAB) [13]. The performance of RED is relative to salinity gradient power and the heat source drives the solutions with different concentrations [14]. Similarly, ammonia concentration difference of TRAB drives by the heat sources but there is no reactive ions transfer caused by salinity gradient inside the battery. The electromotive force of the second type is driven by the temperature difference. Thermally Regenerative Electrochemical Cycle (TREC) [15], Direct Thermal Charging Cell (DTCC) [16] and thermo-galvanic cell [17, 18] are related to the temperature coefficient of electrode potential. Differently, thermo-diffusion cell [19] is related to the Soret effect. TRAB shows overwhelming superiority compared to other techniques in the view of power density. Zhang *et al.* [13] established a TRAB with copper-based redox couples and achieved a power density of 136 W/m^2. Zhu *et al.* [20] and Wang *et al.* [21] then designed a TRAB in flow cell type for continuous operation using copper and zinc achieved the power density to 280 W/m^2 with a corresponding relative efficiency (relative to Carnot efficiency) of 2.7%. From the view of efficiency, TREC and DTCC can potentially achieve a better performance. For example, Lee *et al.* [22] built a TREC system using a copper hexacyanoferrate cathode and a Cu/Cu^{2+} anode and obtained a relative efficiency as high as 38%. Wang *et al.* [16] introduced DTCC and the relative efficiency is 21.4%. However, these techniques are all based on a thermodynamic

cycle which cannot work continuously unless pumps and pipes are added to let the electrolyte flow in a closed loop leading to the difficulty of practical applications. Additionally, electrodes in TRAB and some kinds of TREC participate in the redox reaction so the heat source/sink must switch periodically to reverse the reaction direction, thereby ensuring there is no depletion of the electrode material.

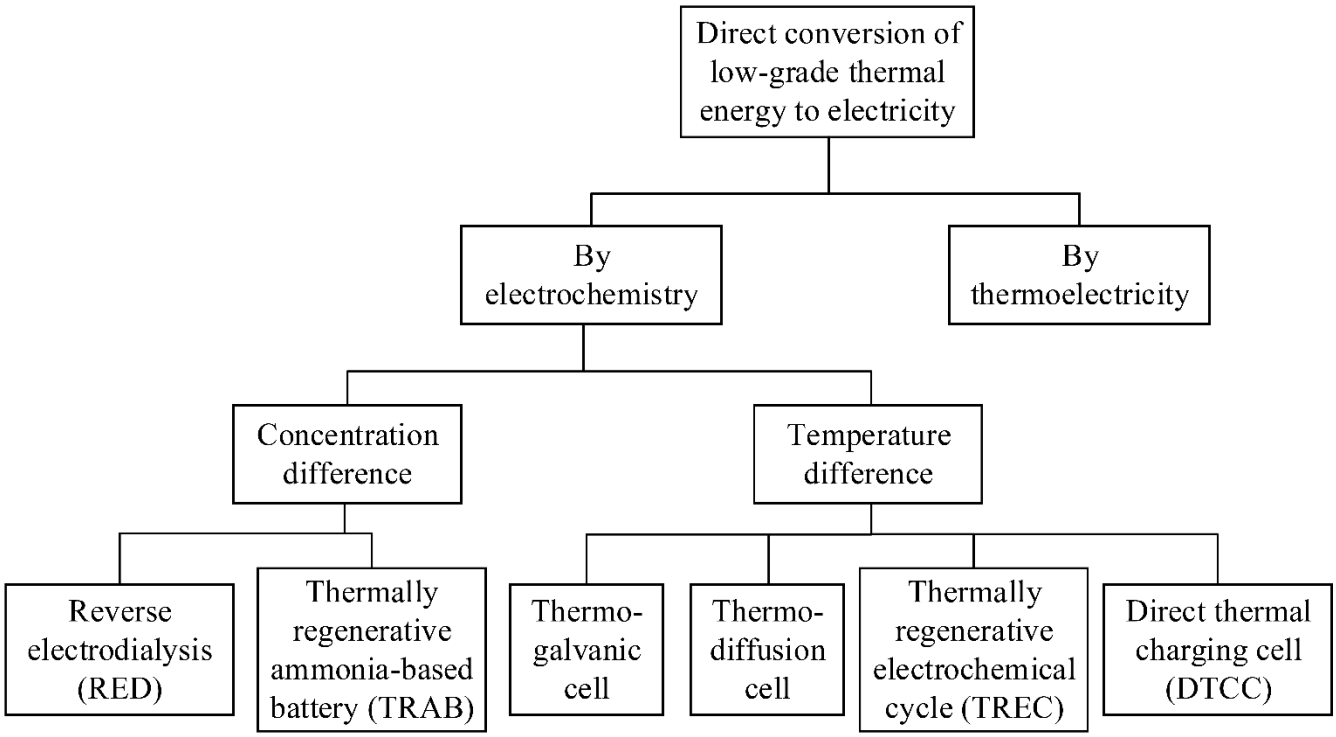

Fig. 1 Classification of techniques for direct conversion of low-grade thermal energy to electricity

Thermo-galvanic cell, also named as thermocell, has a unique advantage among all electrochemical techniques. It is similar to a conventional thermoelectric technique and has the features of high compactness, simple construction with no moving components, and the capability of consecutive operation under temperature difference [23]. Differently, thermocell has a larger Seebeck coefficient (~1 mV/K), which means a higher voltage is acquired [24]. The main component of thermocell is the electrolyte solution and due to its flexible structure, thermocell has been recognised as a promising technology to form a flexible and wearable power system. For instance, Im *et al.* [25] designed a plastic thermocell consisting entirely of flexible materials to use the body heat. Zhou and his group [26, 27] introduced a thermocell with p-n configuration to harvest body heat. Owing to its flexibility, thermocell can be potentially used in curved surfaces such as pipe walls, which are very common in heat recovery energy systems [28, 29]. The other

potential application of this technology is as a replacement of conventional liquid cooling systems with the added benefit for electricity production as reported by Kazim *et al.* [30]. Thermocell has been investigated for over 30 years, however, the low power density and efficiency of the thermocell are the two major limitations restricting its broad utilisation. In 1995, Quickenden *et al.* reported a review article summarising early researches on aqueous thermocell and concluded it was difficult to obtain values over 1.2 % for relative efficiency [31] and the maximum power density was 0.2 W/m^2 [32]. Over the past ten years, the performance of thermocell technology has significantly increased with the progress of material technology. For example, advanced carbon materials, which have outstanding electrochemical performance and relatively good cost performance compared to platinum, were first studied in a thermocell by Hu *et al.* [29] and have been widely investigated. The maximum power density of a thermocell obtained is as high as 12 W/m^2 reported by Zhang *et al.* [33] and the maximum relative efficiency is 3.95 % reported in Ref. [34]. It can be concluded that the thermocell is a very promising solution to be potentially used in practical application with help from extensive technological developments.

Two typical thermocell structures are U-tube cell and straight cell as shown in Fig. 2. The main difference between these two structures is the electrode separation. The U-tube cell [35] has a long curved tube between two electrodes, which effectively diminishes heat transfer and convection in the thermocell. Therefore, the temperature of the electrodes can be accurately controlled. Additionally, the main elements of a U-tube thermocell are available in the laboratory and can be easily assembled without sealing problems. However, the physical structure of the long curved tube greatly increases the internal resistance of the thermocell and the power density is therefore restricted. Conversely, the straight cell [36], whose length can be very small (~mm), can potentially achieve a large power output. Nevertheless, it is difficult to directly measure the temperature at the liquid-solid phase interface where the reaction happens inside the cell. The temperature is instead measured at the outside surface of the straight thermocell unit to approximately back-calculated the temperature inside the cell, which cannot provide precise measurement and control of real temperature difference between electrodes. As reported by Holubowitch *et al.* [37], due to the effect of natural

convection, the temperature difference inside the cell is approximately half of that outside the cell when the cell is established with carbon electrode. The configuration of the straight thermocell needs to be well designed to solve this problem as well as address liquid leakage and convenience of assembly. In summary, it can be concluded that the U-tube cell is more suitable for primary research and accurate measurement of temperature response (Seebeck coefficient) while the straight cell is suitable for achieving high levels of power density and efficiency.

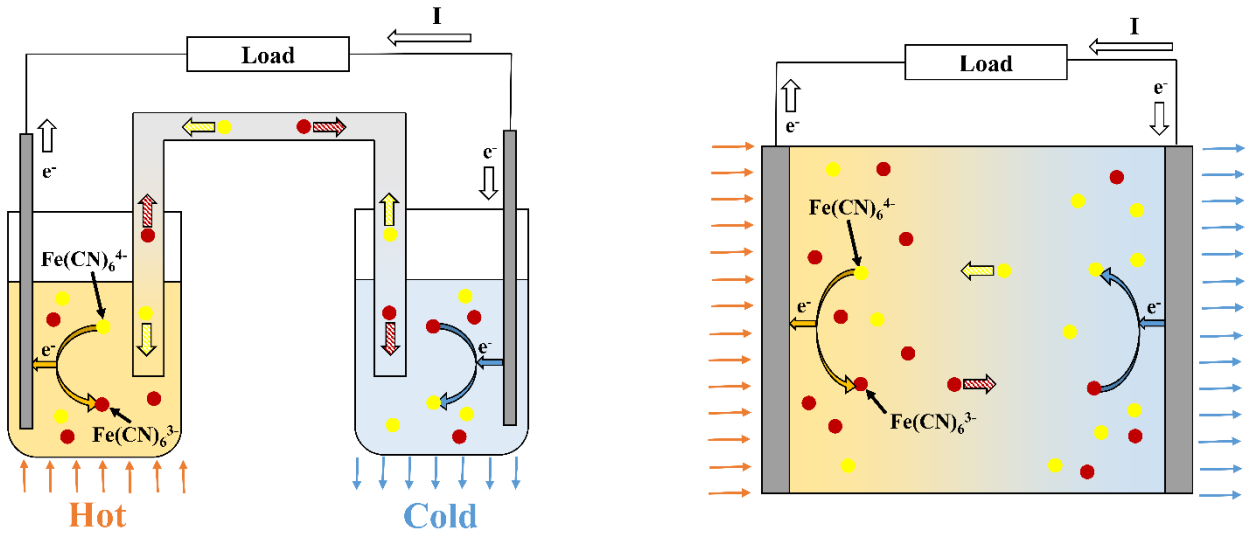

Fig. 2 Schematics of two typical thermocell structures. (a) U-tube cell; (b) Straight cell.

The electrolyte solution is the key component of thermocell, which influences the power density of the system. The solutes determine the redox couple, which significantly affects the Seebeck coefficient. Therefore, it is critical to identify the proper electrolyte solution with a high Seebeck coefficient. The commonly used redox couples in aqueous solutions are $Fe(CN)_6^{3-/4-}$ [32, 33] and $Fe^{2+/3+}$ [38, 39]. The Seebeck coefficients of these are opposite so that they can be designed as p-n type just like a solid thermoelectric generator [40]. To increase the working temperature of thermocell, ionic liquids which have a higher boiling point were adopted as reported in Ref. [41, 42]. For ionic liquids based thermocell, Seebeck coefficients larger than 2 mV/K were obtained [43, 44] and the biggest Seebeck coefficient (7 mV/K) was achieved [45]. Among a large variety of electrolyte solutions, potassium Ferri/ferrocyanide aqueous

solution is the most used due to its ease of availability and low price of the chemicals as well as the high Seebeck coefficient of the redox couple (~1.4 mV/K and a new record of 4.2 mV/K by suitable addictive [46]). The redox couple is $Fe(CN)_6^{3-/4-}$ (Fe3 and Fe4 for short). The increase of solution concentration will lead to an improvement in power density for Fe3/Fe4 thermocell [33]. Additionally, Kang *et al*. [36] found that the open-circuit voltage was enhanced (the Seebeck coefficient grows from 1.43 mV/K to 1.72 mV/K) when the two ion concentrations were reduced from 0.2 mol/L to 0.5 mmol/L. Romano *et al*. [47] found that the thermal conductivity of Fe3/Fe4 solution experienced a slight drop from 0.591 W/m•K to 0.547 W/m•K (both at room temperature) when the total concentration increased from 0.1, 0.1 mol/L to 0.4, 0.4 mol/L.

Electrochemical thermodynamic theory indicates that electrode potential is related to the concentration ratio of redox couple ions in the form of the Nernst equation [48]. Researchers from Kyushu University used a supramolecular technique to alter the concentration ratio of I^-/I_3^- [49] and ferrocenecarboxylate/ferroceniumcarboxylate [50]. The Seebeck coefficients were increased from 0.86 mV/K to 1.97 mV/K and -0.86 mV/K to -1.20 mV/K. Moreover, the solubility of potassium-Fe4 is about half of that of potassium-Fe3 at 0 °C [51] and potassium-Fe4 has one potassium ion more than the other solute. According to the theory of solubility equilibrium, the total concentration of solution can be raised by adjusting the concentration ratio of Fe3/Fe4, reducing the amount of potassium ferrocyanide and meanwhile adding more potassium ferricyanide. However, the effect of concentration ratio on performance of Fe3/Fe4 thermocell is less discussed and concentration ratio of Fe3 and Fe4 in all the research mentioned above is 1:1. Additionally, electrolyte solutions used in thermocell are all concentrated, therefore the ion activity coefficient is necessary for solving the Nernst equation and the solubility product equation. Due to the lack of activity information of potassium-Fe3/Fe4 mixed aqueous solution, theoretical analysis cannot provide a highly accurate result.

In this study, a U-tube thermocell with a specially designed temperature control module is established to study the correlation between the performance of a Fe(CN)63-/4- thermocell and ion concentrations. Firstly, the effects of Fe3/Fe4 concentration on open-circuit voltage, internal resistance and power density have been investigated by the

factorial experiment on the developed U-tube thermocell. Secondly, the dependence of electrode potentials on concentrations and temperatures are obtained by experiment to overcome the lack of data in the literature. Thirdly, the saturation line of electrolyte is obtained to determine the range of concentration using the solubility test. By comparison of experimental and theoretical results, the impact of the activity coefficient on the Nernst equation is proved to be non-negligible and the results demonstrate that neglecting impact on solubility product is acceptable. Finally, the variation of thermocell performance on the saturation line is studied and it is found that power density, efficiency, open-circuit voltage and mass of solutes can be optimised simultaneously.

2. Methodology

2.1 Description of the experimental rig

A U-tube thermocell test rig has been established using a silicone curve tube (~34 cm long, 4 mm inner diameter) to connect two electrolytic glasses, as is shown in Fig. 3 (a). The temperature control module as shown in Fig. 3 (b) consists of thermoelectric coolers (TE Cooler, TEC1-26315), PID thermostat (0.01 °C resolution) and other accessories. With this module, it takes 30 minutes to control the temperature of the electrolyte solution within a less than 0.1 °C fluctuation. Solutions are prepared by volumetric flask with potassium ferricyanide, potassium ferrocyanide trihydrate (CAS No. 13746-66-2, 14459-95-1 respectively, both analytically pure, produced by Hushi Shanghai) and deionized water. The size of a platinum sheet electrode (99.99% pure) is 10*10*0.1 mm. Voltage and current are measured by a six-bit semi-precision digital multimeter (DMM6000, produced by Zhiyuan Electronics Guangzhou) with the red pen linked to the hot electrode and the black pen linked to the cold electrode during the test. The sampling frequency and time are 2.5 Hz and 10 min. In each measurement, sampling data is verified by a 3-sigma rule before calculating the mean value as the final value and setting a waiting time of one hour to ensure the temperature and measured data are stable. Fig. 3 (c) shows the integrated apparatus for this experiment.

(a)

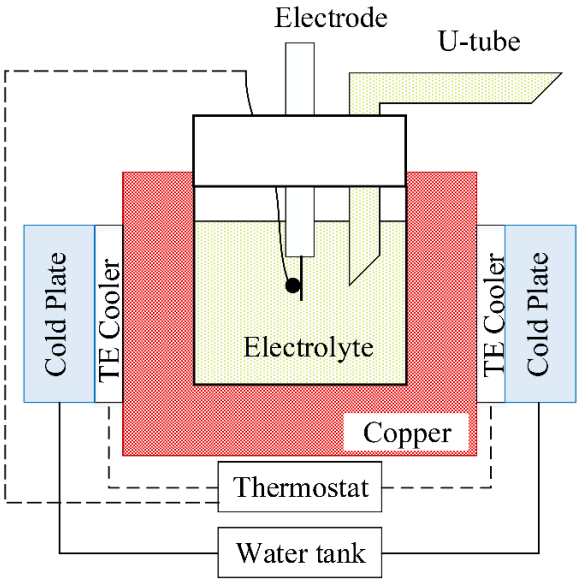

(b)

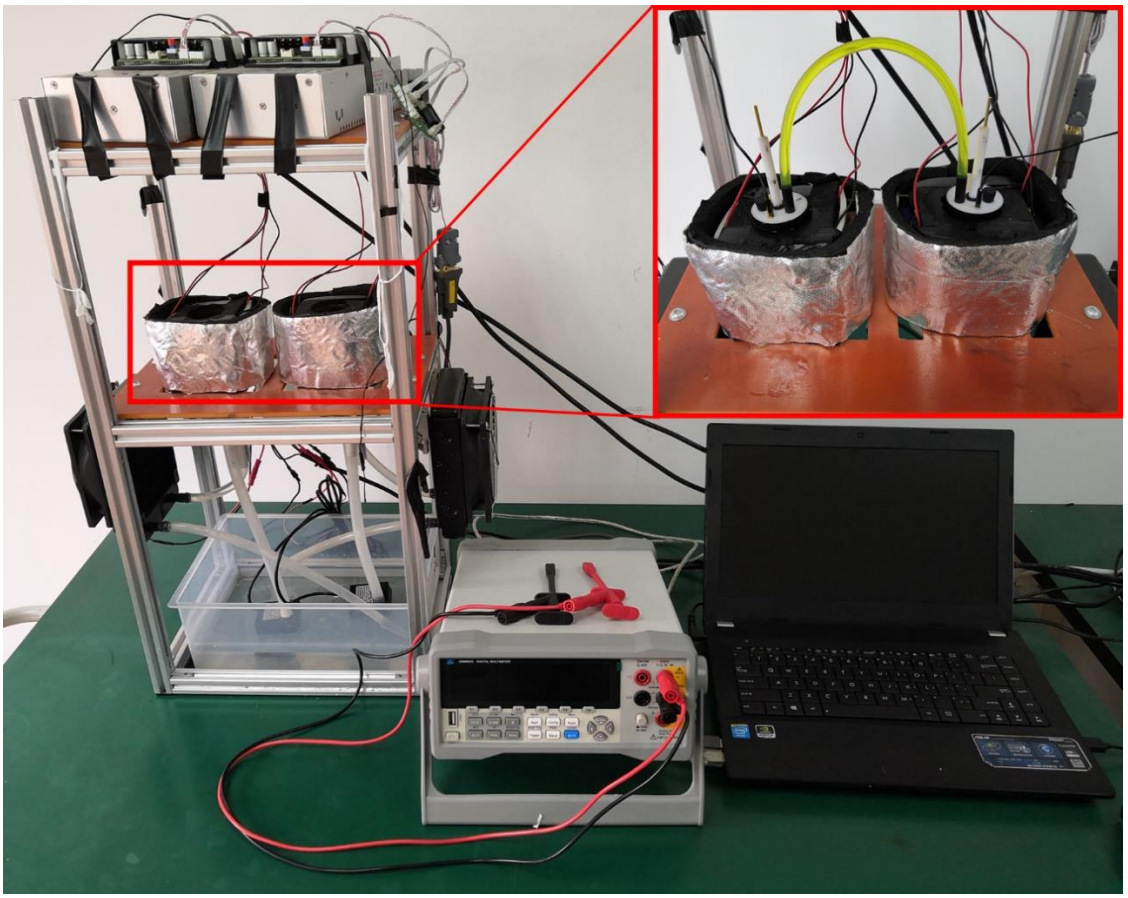

(c)

Fig. 3 (a) An assembled U-tube thermocell adopted in this paper; (b) Schematic diagram (a symmetric half) of the temperature control module; (c) Picture of the integrated apparatus.

The U-I plot of thermocell is found to be linear as reported in references [31, 36], so that maximum power density and internal resistance of thermocell can be calculated as Eq. (1) and Eq. (2), where P_{max} is maximum power density, A is the area of the electrode (two sides, 200 mm^2) and R_{int} is internal resistance. U_{oc} and I_{sc} are open-circuit voltage and short-circuit current, which are measured directly by a multimeter.

$$P_{max} = 0.25U_{oc}I_{sc}/A = 0.25U_{oc}^2/(R_{int}A) \quad (1)$$

$$R_{int} = U_{oc}/I_{sc} \quad (2)$$

For the factorial experiment, the concentrations of Fe3 and Fe4 are the factors to be studied and each concentration has three levels: 0.1 mol/L, 0.25 mol/L and 0.4 mol/L. Each experiment is repeated independently three times to analyse the interaction effect of two factors and experimental error. To reduce the relative error of measurement, the temperature difference should be large enough. Therefore, in the experiments, the hot side is set to 70 °C to limit the evaporation of the solution. The cold side is set to 15 °C because precipitation occurs in the most concentrated solution (0.4, 0.4 mol/L) at 10 °C, which makes the actual concentration smaller than the original value. Data will then be treated by analysis of variance (ANOVA for short) and analysis of regression (ANORE for short) to present the influence on thermocell performance.

The temperature of the ice-water mixture is selected for the solubility test and, in practice, the measured temperature is in the range of 1-3 °C. The concentration interval is 0.05 mol/L. The test is conducted in the order of pure potassium ferrocyanide solution, 1:1 concentration ratio solution, and the vicinity of the line connecting two critical saturated points above. Each test has a 5 hour waiting time to allow the solution to approach solubility equilibrium.

2.2 Theoretical analysis

The electrode potential of Fe3/Fe4 is determined by the Nernst equation as shown in Eq. (3), where φ is the electrode potential, φ_f is the formal potential of an electrode, R and F are the gas constant and Faraday's constant, T is the electrode temperature, C_{Fe3} and C_{Fe4} are the concentration of Fe3/Fe4. Formal potential can be written as Eq. (4),

where φ^0 is the standard electrode potential at T_0 which is the standard temperature and is normally 298.15 K, α is the temperature coefficient of φ^0, γ is the activity coefficient. According to thermodynamics of electrochemistry, α is calculated by Eq. (5) [48], where ΔS^0 is the entropy change of reaction under a standard state. As it is known that electrode potential is normally defined against hydrogen standard electrode potential, Eq. (5) can be calculated based on the reaction of $Fe(CN)_6^{3-} + 1/2H_2 = Fe(CN)_6^{4-} + H^+$. Thermodynamic data of each chemical substance is listed in Table 1. The results are -2.503 mV/K and -2.494 mV/K by formation entropy and conventional entropy respectively, therefore α = -2.5 mV/K. It is larger than the value of ~1.4 mV/K reported in an early study, which indicates the influence of ion activities.

$$\varphi = \varphi_f + (RT/F)\ln(C_{Fe3}/C_{Fe4}) \quad (3)$$

$$\varphi_f = \varphi^0 + \alpha(T\text{-}T_0) + (RT/F)\ln(\gamma_{Fe3}/\gamma_{Fe4}) \quad (4)$$

$$\alpha = \partial\varphi^0/\partial T = \Delta S^0/F \quad (5)$$

Table 1 Standard Thermodynamic data from the CRC Handbook of Chemistry and Physics [51].

Substances	$\Delta_f H^0$ **(kJ/mol)**	$\Delta_f G^0$ **(kJ/mol)**	$\Delta_f S^0$ [1] **(J/(mol K))**	S^0 **(J/(mol K))**
$Fe(CN)_6^{3-}$(aq)	561.9	729.4	-561.8	270.3
$Fe(CN)_6^{4-}$(aq)	455.6	695.1	-803.3	95.0
H^+(aq)	0	0	0	0
H_2(g)	0	0	0	130.680

[1] Formation entropy is calculated in light of $\Delta_f S^0 = (\Delta_f H^0 - \Delta_f G^0)/T$.

Due to the existence of a long curved tube, the influence of the Soret effect can be ignored. Soret effect is a mass transport phenomenon induced by the temperature difference, which forms a concentration gradient in solutions. The time for establishing a stable Soret phenomenon is determined by Eq. (6) [52], where τ is the characteristic time, d is the separation of electrodes and D is the diffusion coefficient of ion. D is about ~10^{-5} cm^2/s for ions in aqueous

solutions and Fig. 4 shows the dependence of τ on d at different D. It is found that when the distance of electrodes is greater than 5 cm, it will take more than a day to observe the Soret effect. For Fe3 and Fe4, D is less than 3×10^{-5} cm^2/s in the temperature range of 10-90 ° C [53]. In this paper, the length of the tube is 34 cm and characteristic time is greater than one month. Therefore in the period of the experiment, the Soret effect is negligible and open-circuit voltage is equal to the difference value of two electrode potentials as presented in Eq. (7). Moreover, the long curved tube hinders the formation of natural convection and the heat transferred through thermocell can be regarded as heat conduction. Here heat conduction in a curved tube is simplified as a straight tube and it is determined by one dimensional Fourier equation written as Eq. (8), where q is the heat flux, k is the thermal conductivity.

$$\tau = d^2/(\pi D) \tag{6}$$

$$U_{oc} = \Delta\varphi = \alpha\Delta T + \Delta[(RT/F)\ln(\gamma_{Fe3}/\gamma_{Fe4})] + (R\Delta T/F)\ln(C_{Fe3}/C_{Fe4}) \tag{7}$$

$$q = -k(dT/dx) \tag{8}$$

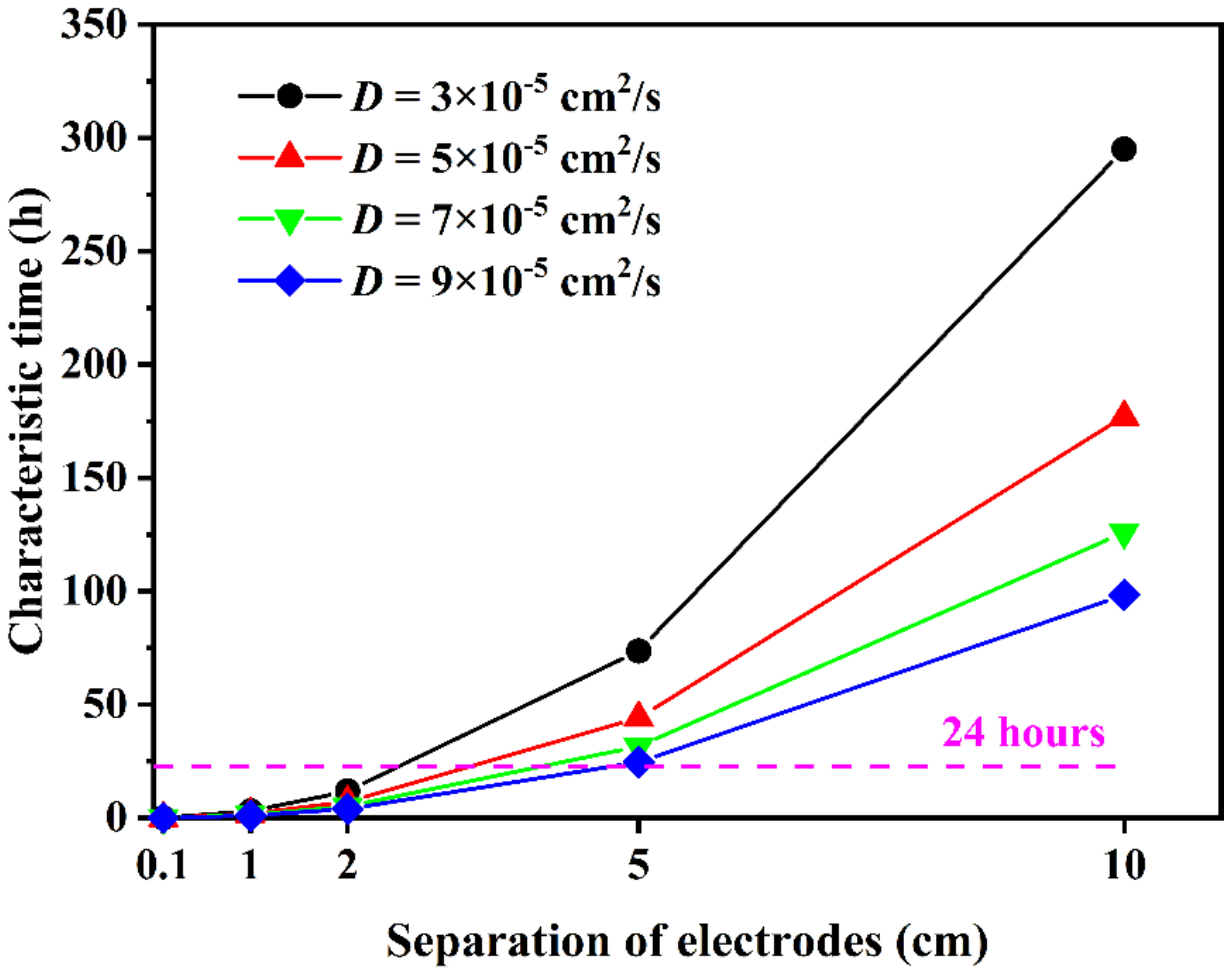

Fig. 4 Dependence of characteristic time on the separation of electrodes at different diffusion coefficients.

Activity solubility product $K_{sp\text{-}a}$ is a constant at a fixed temperature and when compared to the concentration solubility product, the difference is the activity coefficient product K_γ (see Eq. (9) and Eq. (10)) whose accurate value is difficult to determine in a concentrated mixed solution. Nevertheless, if K_γ does not vary with concentration, K_{sp}-c can be treated as a constant at a fixed temperature. Because potassium ions are all from the two solutes, the concentration of Fe3 and Fe4 will be related as Eq. (11).

$$K_{sp\text{-}a} = a_K^4 a_{Fe4} = K_\gamma C_K^4 C_{Fe4} \quad (9)$$

$$K_{sp\text{-}c} = C_K^4 C_{Fe4} \quad (10)$$

$$3C_{Fe3} = (K_{sp\text{-}c}/C_{Fe4})^{0.25} - 4C_{Fe4} \quad (11)$$

3. Results and discussion

3.1. Factorial experiment

To show the overall dependence of Fe3/Fe4 concentrations on the performance of thermocell, main effect plots and contour plots are presented in Fig. 5. Contour plots are plotted according to the results of ANORE. The multiple correlation coefficients of open-circuit voltage, internal resistance and power density are 0.9997, 0.9889 and 0.9995 respectively. Results of ANOVA for experimental data are listed in Table 2. All F-values are larger than $F_{0.01}$, therefore the effects of factors in the table are very significant and the experiment has sufficient precision to reveal the influence of concentration.

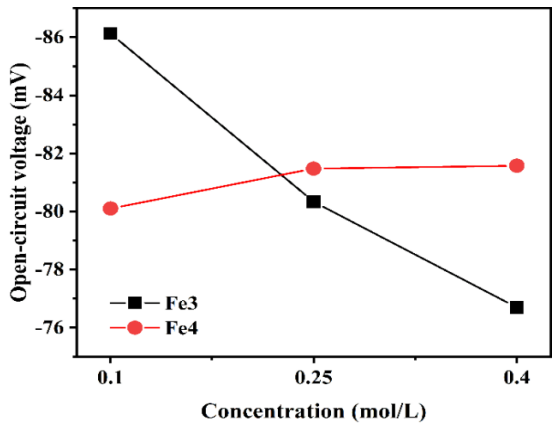

(a)

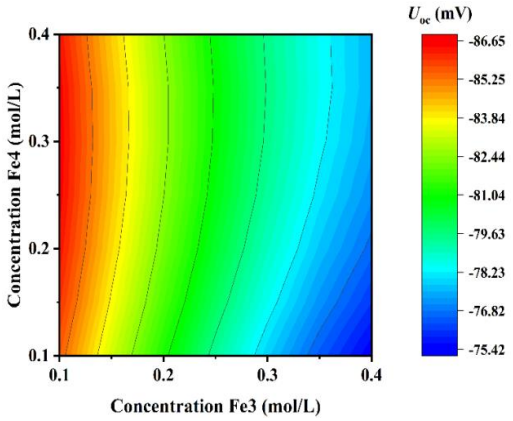

(b)

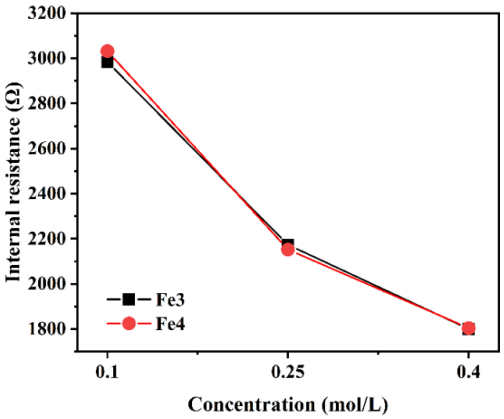

(c)

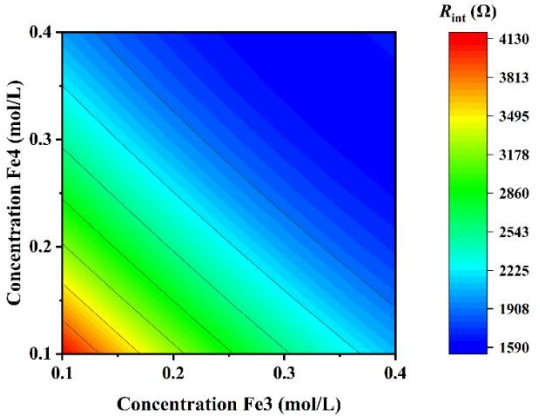

(d)

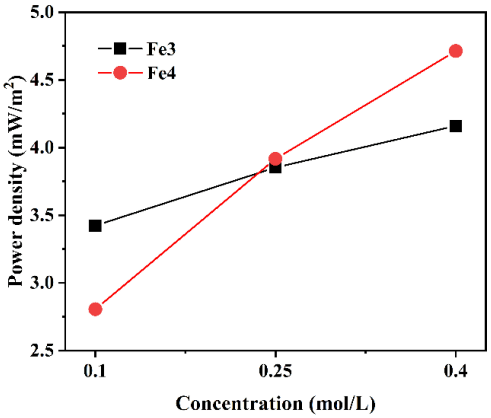

(e)

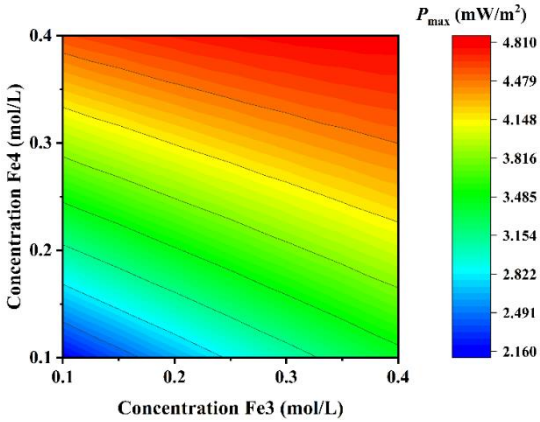

(f)

Fig. 5 Dependence of thermocell performances on Fe3/Fe4 concentrations. Main effect plots for (a) open-circuit voltage, (c) internal resistance and (e) power density; (b) (d) (f) Contour plots for these three performance indexes.

Table 2 Results of ANOVA.

Factors	*df*	*F-U_{oc}*	*F-R_{int}*	*F-P_{max}*	*$F_{0.01}$*
Fe3	2	10263.6	6480.63	980.959	6.01291
Fe4	2	307.783	7385.71	6573.92	6.01291
Fe3×Fe4 (Note)	4	18.7005	1252.77	159.256	4.57904
Error	18				

(Note) Interaction effect of Fe3/Fe4 concentration.

3.1.1 Open-circuit voltage

Fig. 5 (a) shows two opposite variation tendencies on open-circuit voltage with different extents. The average voltage reduces by 11% with the increase of Fe3 concentration while it grows by less than 2% with the increase of Fe4 concentration. ANOVA in Table 2 shows the same result in a quantitative manner, where the effect of Fe3 is about 33 times larger than that of Fe4. Thus by rough approximation, it can be concluded that the open-circuit voltage is only related to the concentration of Fe3 and the greater concentration will result in a lower value of voltage. This conclusion can also be drawn from Fig.5 (b), where the contour line is nearly perpendicular to the horizontal axis, especially in the upper half section (Fe4 > 0.25 mol/L region).

In light of Eq. (7), if the effect of the activity coefficient is ignorable, the equation can be simplified as Eq. (12), where both the activity coefficients are 1 (ideal situation). Fig. 6 (a) and Fig. 6 (b) show the comparison of theoretical and experimental values. Because the concentration of Fe3 and Fe4 are positioned at the numerator and denominator of the antilogarithm respectively, the dependence of Fe3/Fe4 concentration on open-circuit voltage should be symmetrically opposite and the voltages at 1:1 points ought to be the same. However, the experimental results are significantly different from the theoretical results. Firstly, the experimental values are smaller than the calculated values; the experimental values are approximately 60 % of the calculated values. Consequently, the variation tendency is no longer symmetrical,

which makes the voltage at 1:1 points reduce with an increase of total concentration. Also, according to Eq. (12) the effects of Fe3 and Fe4 on open-circuit voltage should be completely independent and that is why in Fig. 6(a), (b), variations of theoretical values are paralleled. From the F-value of Fe3×Fe4 and the variations of experimental values, the same result is observed and the interaction effect of Fe3/Fe4 on open-circuit voltage is negligible. Therefore, the existence of activity coefficients reduces open-circuit voltage significantly and changes the dependence of open-circuit voltage on concentration but has almost no influence on the interaction effect of Fe3/Fe4.

$$U_{oc} = \Delta\varphi \approx \alpha\Delta T + (R\Delta T/F)\ln(C_{Fe3}/C_{Fe4}) \quad (12)$$

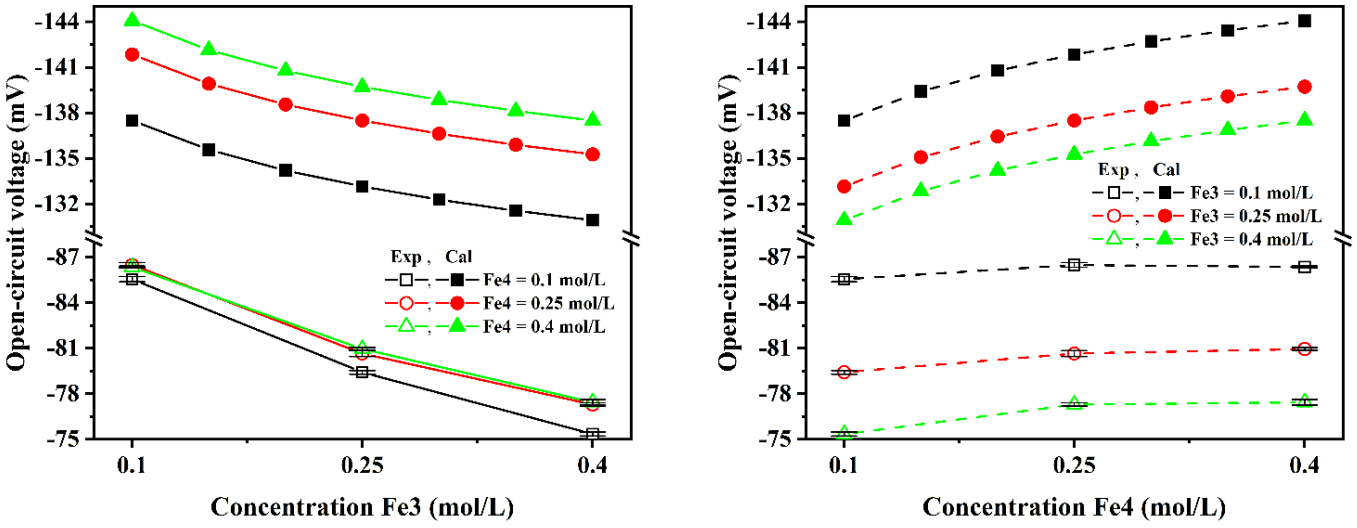

(a) (b)

Fig. 6 Comparison of theoretical and experimental values by interaction plots. (**a**) Fe4 concentration fixed; (**b**) Fe3 concentration fixed. The green dash lines connect the points with a concentration ratio of 1:1. All errors here are standard deviations.

3.1.2. Internal resistance

The internal resistance can be approximately recognised as the ohmic resistance in U-tube thermocell due to its large distance of electrodes [32]. The ohmic resistance is determined by electric conductivity which is relative to the ion concentration for a specified cell structure. As shown in Fig. 5 (c), the influences of Fe3/Fe4 concentrations on internal resistance are almost the same. The contour lines in Fig. 5 (d) are straight with a ~135° slope. It is therefore feasible to

assume that the ohmic resistance is only related to total concentration. Fig. 5 (c) shows that in the studied range, increasing either Fe3 or Fe4 will lead to a 40% drop in average ohmic resistance. ANOVA result in Table 2 shows that the influence of Fe4 is slightly greater than that of Fe3 because potassium-Fe4 has one potassium ion more than potassium-Fe3. Additionally, the interaction effect between two kinds of ions should not be neglected because its F-value has the same order of magnitude as Fe3 and Fe4. Fig. 7 is the interaction plot of Fe3/Fe4 concentrations on internal resistance, and it is found that when the concentration of Fe4 is 0.4 mol/L, the decrease of internal resistance induced by the growth of Fe3 concentration is much less pronounced. It results from the decline of equivalent conductivity when the total concentration of the solution increases. Also, there is still a potential to decrease ohmic resistance but the effect of adding more solutes will not be apparent.

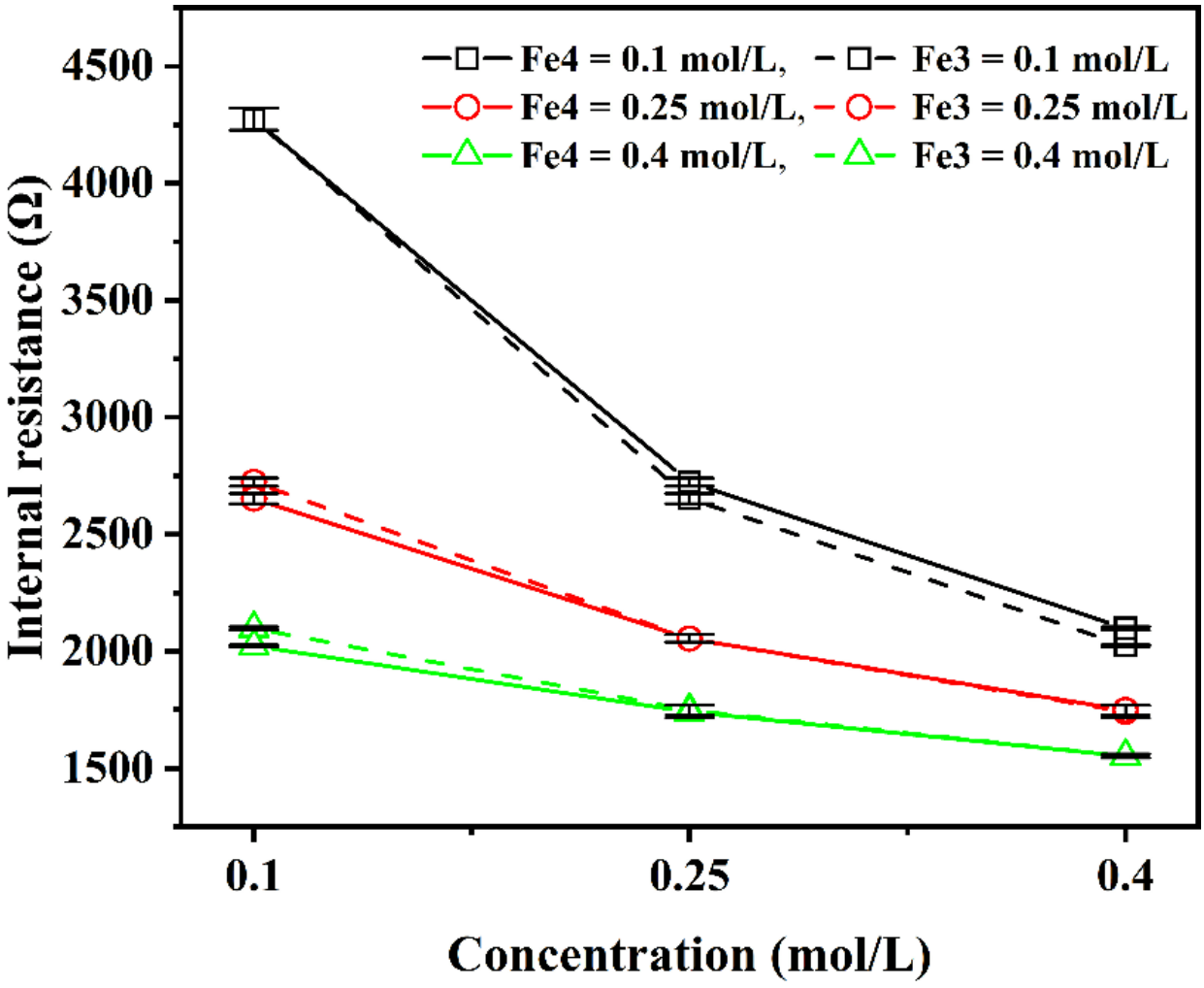

Fig. 7. Interaction plot of Fe3/Fe4 concentrations on internal resistance.

Note: Errors in this figure are within standard deviations.

3.1.3. Maximum power density

The power density is determined by the open-circuit voltage and internal resistance which are dependent on the concentration of Fe3 and Fe4, as described in Eq. (1). Also, the concentration of Fe4 is considered to only influence internal resistance as is previously discussed, hence power density is positively related to Fe4 concentration. The concentration of Fe3 has opposite influence on open-circuit voltage and internal resistance, but the overall effect on power density is still positive. As is shown in Fig. 5(e), average power density grows 21.5% and 68.0% through increasing the concentration of Fe3 and Fe4. ANOVA results show that the extent of influence of Fe4 is 6-7 times that of Fe3. Therefore, raising the concentration of Fe3 and Fe4 is an effective way of improving power density and Fe4 plays a more significant role. In the studied range, the power density under the most concentrated condition is 2.26 times the level of that under the most dilute condition. The interaction effect is not substantial but from interaction plot Fig. 8, it is shown that when Fe4 is 0.4 mol/L, Fe3 has almost no influence on the power density.

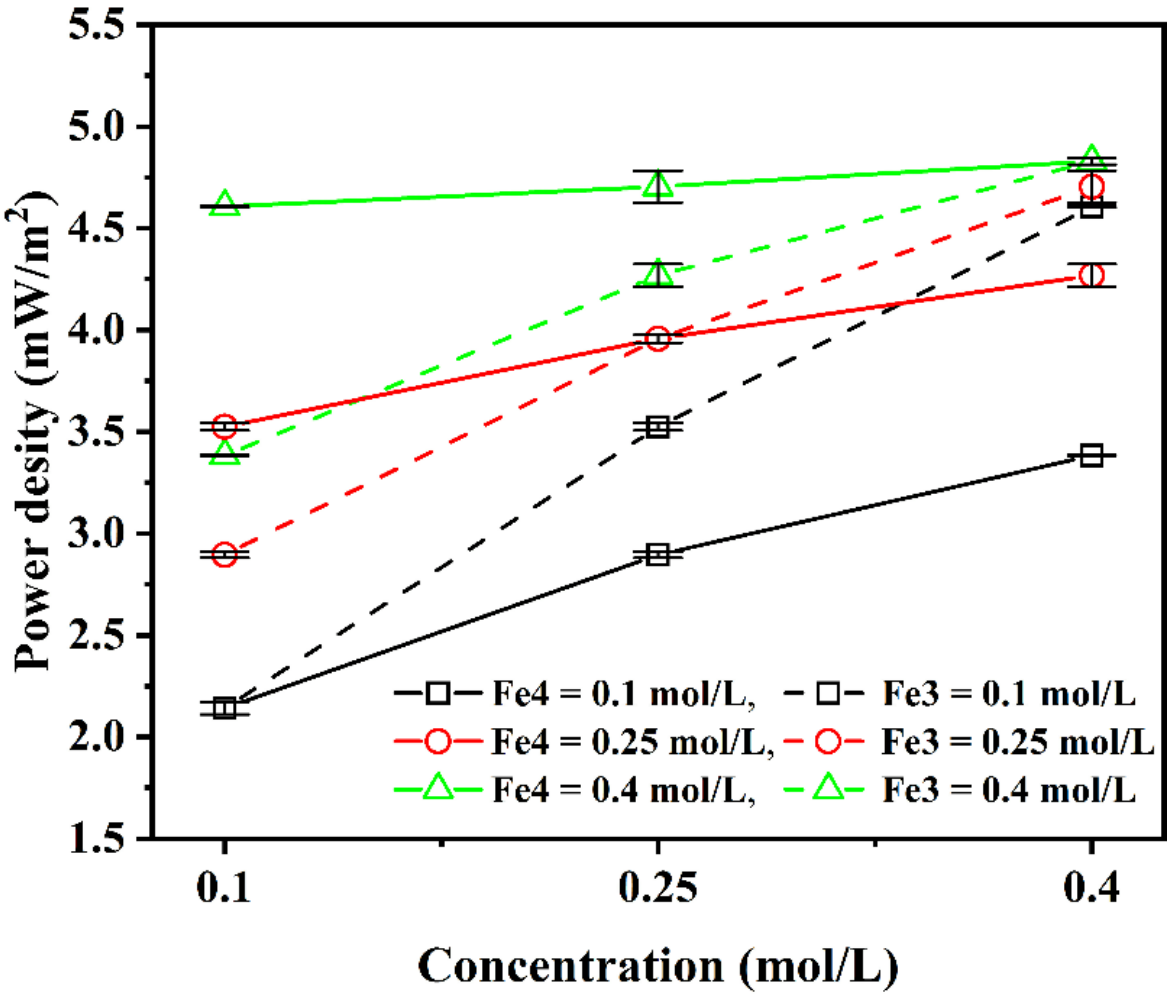

Fig. 8 Interaction plot of Fe3/Fe4 concentrations on power density. All errors here are standard deviations.

3.2 Electrode potentials

Due to the lack of activity coefficient data, the Nernst equation cannot accurately describe electrode potentials. Thus, the measurement of electrode potentials at 25 °C is conducted by the same experimental facility but only half of the apparatus is used in order to keep the temperature of solution constant. The reference electrode adopted here is Ag/AgCl (saturated) whose electrode potential at 25 °C is about 197 ± 3 mV against standard hydrogen electrode. According to Eq. (3) and (4), electrode potential can be divided into four parts: standard electrode potential, φ^0, which is 361.0 mV for the studied reaction [48]; temperature term, $\alpha(T\text{-}T_0)$, where α is -2.5 mV and T_0 is 298.15 K; activity coefficient term, $(RT/F)\ln(\gamma_{Fe3}/\gamma_{Fe4})$; concentration term, $(RT/F)\ln(C_{Fe3}/C_{Fe4})$. Therefore, the activity coefficient term can be calculated by subtracting the other three terms from electrode potential.

The results of electrode potential measurements are presented in Fig. 9 and the values are greater than 361 mV, and this is caused by concentration term and activity coefficient term. To show the effect of activity coefficient, activity coefficient terms and their proportions in electrode potentials are calculated and this data is presented in Fig. 9 (a). Approximately 20%-25% of the electrode potential is composed of the activity coefficient term, which again illustrates the importance of activity coefficients in the Nernst equation. Additionally, from Fig. 9 (b), it is found that the activity coefficient term not only changes the amount of electrode potential but also changes its distribution. At a certain ratio of Fe3/Fe4 concentrations, the electrode potential rises with the increase of total concentration of electrolyte solution.

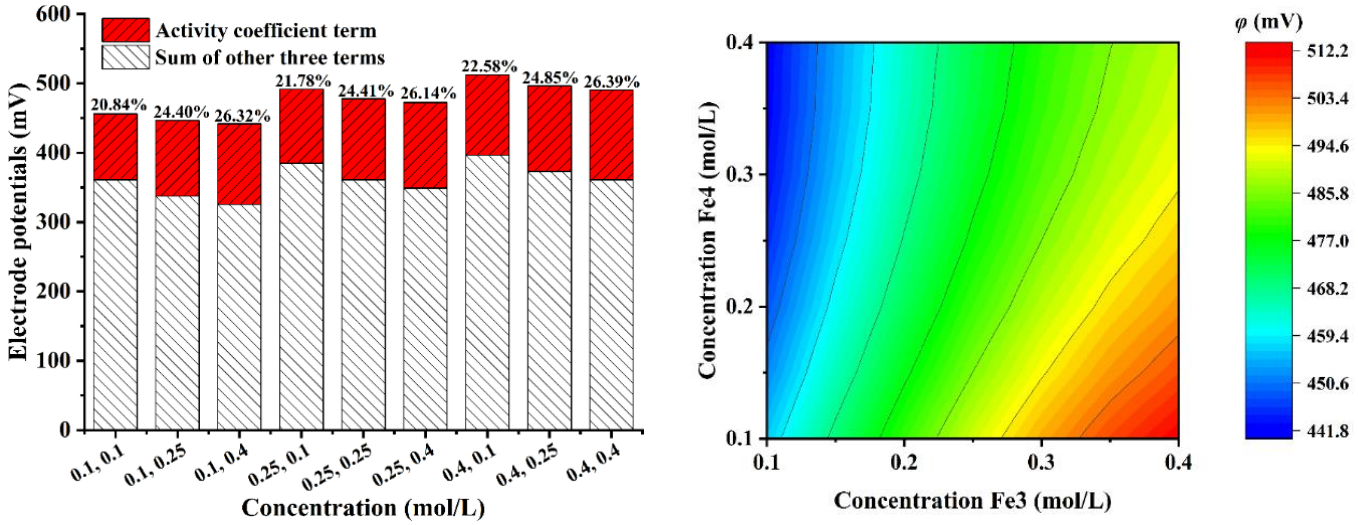

(a) (b)

Fig. 9. (**a**) Electrode potentials and proportions of activity coefficient terms at different concentrations. Maximum standard deviation is 0.27% of the measured value; (**b**) Contour plot for electrode potentials.

Electrode potential is a necessary parameter in the computation of electrode kinetics. Therefore, the dependence of electrode potential on concentration and temperature in the whole studied range should be determined. The dependence of electrode potential on the concentration at 25 °C is shown as Eq. (13), which is the result of ANORE. The multiple correlation coefficient is 0.9997 and the maximum residual is 0.22% of the measured value. From the earlier research, it is found that when the electrolyte of the solution is at a certain concentration, the open-circuit voltage is linear to temperature difference [29, 36], which means the Seebeck coefficient is independent of temperature. Thus, the

dependence of electrode potential on temperature can be written as Eq. (14), where α_S is the measured Seebeck coefficient. α_S can be calculated by dividing the measured open-circuit voltages with the temperature difference 55 °C, and the dependence of α_S on concentration can be obtained by ANORE and is shown as Eq. (15). The corresponding multiple correlation coefficient is 0.9997 and the maximum residual is 0.23% of the measured value. According to Eq. (13)-(15), electrode potential at any temperature and concentration can be predicted.

$$\varphi_{25°C} = 437.453 + 341.590C_{Fe3} - 128.554C_{Fe4} - 296.955C_{Fe3}^2 + 175.151C_{Fe4}^2 - 82.836C_{Fe3}C_{Fe4}, \quad (13)$$

$$\varphi = \varphi_{25°C} + \alpha_S(T - 298.15) \quad (14)$$

$$\alpha_S = 1.6274 + 1.0700C_{Fe3} - 0.2799C_{Fe4} - 0.8657C_{Fe3}^2 + 0.5120C_{Fe4}^2 - 0.2622\,C_{Fe3}C_{Fe4} \quad (15)$$

3.3. Solubility test and calculation

Fig. 10 demonstrates the results of the solubility test. Solid points with plus symbols show that at this concentration, the solution is saturated and the quantity of plus symbols represents the amount of precipitation. Hollow points mean that there is no precipitation observed in the test. A fitted line of four hollow points is presented in Fig. 10 to roughly show the saturation line and the intersection point with 1:1 line is 0.32, 0.32 mol/L, which can be treated as a critical saturated point when the ratio of Fe3/Fe4 concentration is 1:1. According to Eq. (10), $K_{sp\text{-}c}$ at ~2 °C is approximately 8, and the calculated saturation line at $K_{sp\text{-}c} = 8$ by Eq. (11) is shown in Fig. 10 as the green line. The calculated saturation line does not strictly correspond to the actual situation but it can show the distribution of critical saturated points. It means that the activity coefficient product K_γ in Eq. (9) can be treated as constant to some extent. When no further accurate data is available, the saturation line calculated from $K_{sp\text{-}c}$ is a good approximation.

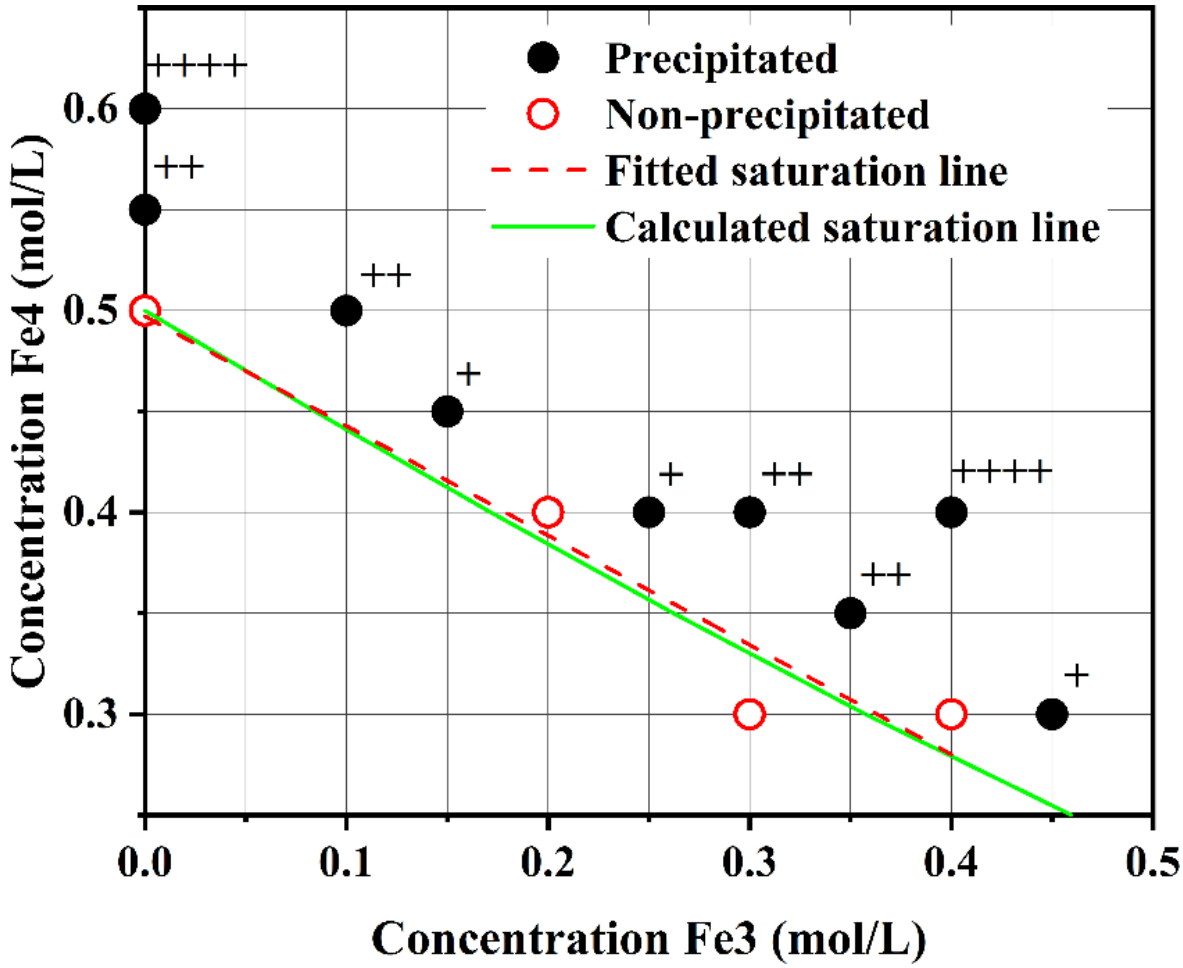

Fig. 10 Results of the solubility test and the calculated saturation line. "+": several grains; "++": dozens of grains; "++++": the bottom is covered by deposits.

3.4. Performance of thermocell on the saturation line

In light of Eq. (11) the variation of Fe3/Fe4 concentration on the saturation line is presented in Fig. 11. Concentrations of Fe3 and Fe4 are conflicting but the slope (absolute value) of Fe3 is larger and therefore total concentration grows when the concentration of Fe3 increases. Growth of total concentration is beneficial for power density because it reduces the internal resistance. However, the increase of Fe3 will reduce the open-circuit voltage which is contrary to the improvement of power density.

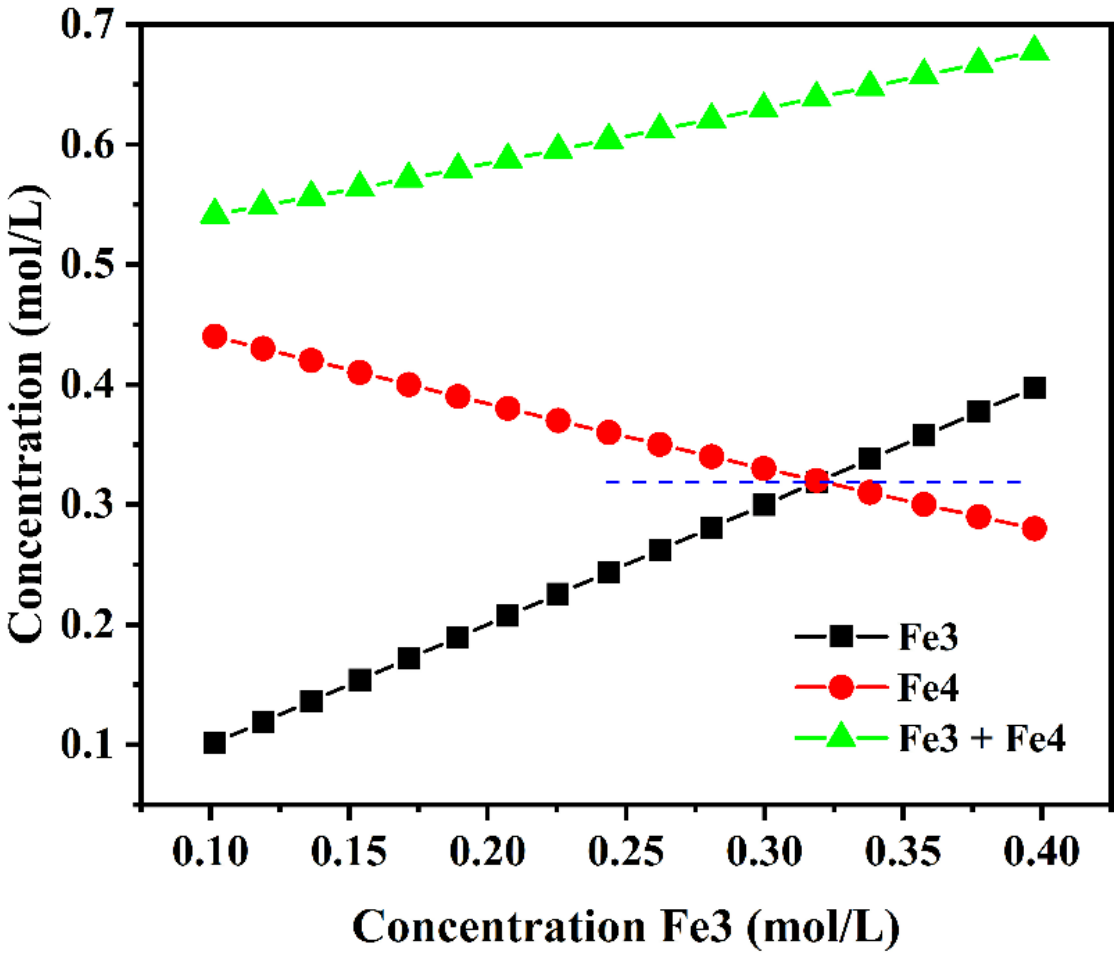

Fig. 11 Concentration variation on saturation line (at $K_{sp\text{-}c}$ = 8)

To reveal the variation of power density on the saturation line, ANORE is conducted using experimental data. Eq. (16) is regression equation of power density. The multiple correlation coefficient is 0.9995 and the maximum residual is 1.68% of the measured value. Fig. 12 (a) is the contour plot of power density with the saturation line shown on the figure. It is found that with the increase of Fe3 on the saturation line, power density declines, which means the reduction of open-circuit voltage has a greater influence than the reduction of internal resistance. Solving Eq. (11), (15) and (16) to obtain the variation of power density and Seebeck coefficient on the saturation line. Mass of solutes in one unit electrolyte solution (1 L) is also calculated. Results are shown in Fig. 12 (b) and it is found that by decreasing the amount of Fe3, both power density and Seebeck coefficient increase, while the mass of solutes decreases. This demonstrates that the optimisation of thermocell performance and material cost are achieved simultaneously by decreasing Fe3.

$$P_{max} = 0.4418+6.6280C_{Fe3}+12.6820C_{Fe4}-2.6843C_{Fe3}^{2}-6.9908C_{Fe4}^{2}-11.3214C_{Fe3}C_{Fe4}, \quad (16)$$

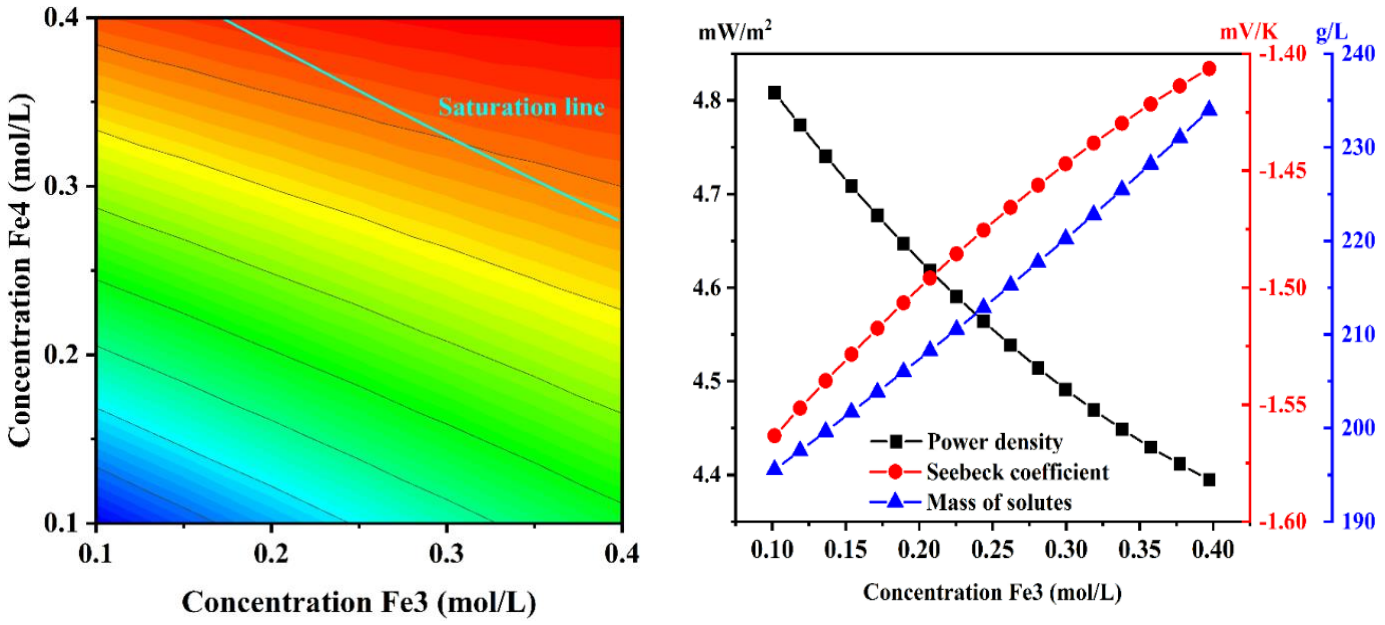

(a) (b)

Fig. 12 (a) Saturation line in the contour plot of power density. **(b)** Variation of power density, Seebeck coefficient and mass of solutes on the saturation line.

Concentration points 0.1, 0.44 mol/L and 0.32, 0.32 mol/L are chosen for a performance test, and the results are listed in Table 3. The prediction of regression is reliable and compared to the 1:1 concentration point, maximum power density increases by 7.38%, Seebeck coefficient increases by 8.93 % and the mass solute decreases by 12.64%.

Table 3 Comparison of thermocell performance (0.1, 0.44 and 0.32, 0.32 mol/L).

	t-P_{max} [1] (mW/m^2)	rp-P_{max} [2] (mW/m^2)	t-α_S (mV/K)	rp-α_S (mV/K)	Mass (g/L)
0.1, 0.44 mol/L	4.8145	4.8063	-1.5730	-1.5646	195.02
0.32, 0.32 mol/L	4.4835	4.4710	-1.4440	-1.4376	223.24
Percentage of increasing	7.38%	7.50%	8.93%	8.83%	-12.64%

Note:[1] t: test value; [2] rp: regression predictive value.

Energy conversion efficiency is the ratio of power density and heat flux through thermocell. To estimate the difference of heat fluxes at 0.1, 0.44 mol/L and 0.32, 0.32 mol/L, thermal conductivity k is needed to solve Eq. (8). Thermal conductivities of electrolyte solutions with 1:1 concentration ratio were measured by Romano *et al.* [47]. Data is replotted in Fig. 13. Fig. 13(a) shows that thermal conductivity is linear to total concentration at 1:1 concentration ratio

(R squares are larger than 0.99) and the slopes at different temperatures are almost the same. It is known from the previous discussion that Fe3/Fe4 concentrations have a similar effect on electric conductivity and here we assume that the contribution of Fe3/Fe4 concentrations to thermal conductivity is also the same, which means the thermal conductivity is linear to total concentration with any ratio of concentration. Total concentration of 0.1, 0.44 mol/L and 0.32, 0.32 mol/L are 0.54 mol/L and 0.64 mol/L. The corresponding thermal conductivities at different temperatures are obtained from linear fitting equations. Results are presented in Fig. 13 (b). Dependence of thermal conductivity on temperature is nearly linear with the R squares larger than 0.97. According to Eq. (8), it can be proved that heat flux is determined by Eq. (17) in one-dimensional heat conduction when thermal conductivity is linear to temperature. T_1, T_2 are the temperatures of cold and hot sides. k_1 and k_2 are thermal conductivities at T_1 and T_2. L is the distance of hot and cold sides. Therefore, the ratio of heat fluxes at 0.1, 0.44 mol/L and 0.32, 0.32 mol/L is the ratio of corresponding $k_1 + k_2$. The value is 1.0160, indicating that the heat flux at 0.1, 0.44 mol/L is 1.60 % more than that at 0.32, 0.32 mol/L. Considering both the growth of power density and heat flux, efficiency is increased by 5.69 %.

$$q = -0.5(k_1 + k_2)(T_2 - T_1)/L \tag{17}$$

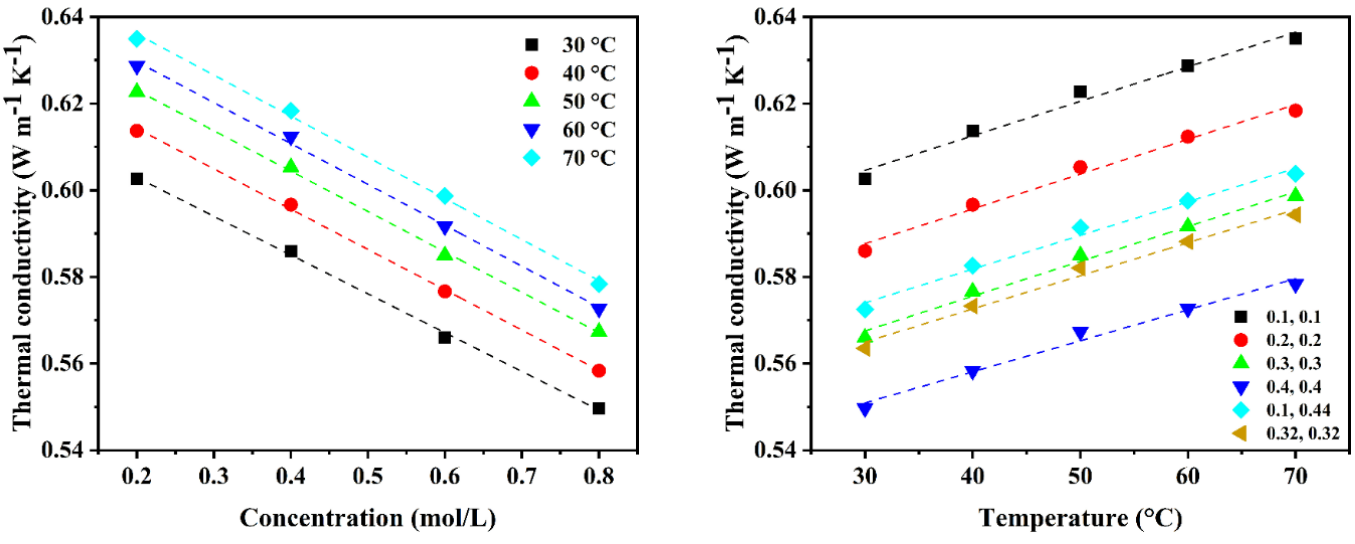

(a) (b)

Fig. 13 (a) Dependence of thermal conductivity on concentration at different temperatures. **(b)** Dependence of thermal conductivity on the temperature at different concentrations.

4. Conclusions

This paper reports a study regarding the influence of $Fe(CN)_6^{3-/4-}$ concentrations on the performance of a U-tube thermocell by experimental and theoretical analysis for further improvement of thermocell performance. Open-circuit voltage, internal resistance, power density, electrode potential and solubility are investigated. The main conclusions are presented below:

(1) Concentrations of Fe3/Fe4 have a significant effect on open-circuit voltage, internal resistance and power density. Open-circuit voltage can be approximately considered as only relative to the concentration of Fe3 and increasing Fe3 will decrease voltage. Concentrations of Fe3 and Fe4 have the same influence on ohmic resistance and raising concentration can effectively reduce ohmic resistance. Taken together, raising the concentration of Fe3 or Fe4 is beneficial for improving power density and the effect of Fe4 is greater.

(2) Activity coefficient has different degrees of effect on the calculation of the Nernst equation and solubility product. It plays a very important role in the Nernst equation, and the activity coefficient term is over 20% of the electrode potential. However, the activity coefficient product could be treated as constant to some extent. Therefore, the saturation line calculated from the concentration solubility product is a good approximation when very limited accurate data is available.

(3) On the saturation line, total concentration can be raised by increasing Fe3 and decreasing Fe4. Nonetheless, this does not improve power density for the decline of the open-circuit voltage induced by the growth of Fe3. However, adjusting the concentration of Fe3 and Fe4 to the opposite direction shows promising results, where power density, Seebeck coefficient, efficiency and mass of solute is simultaneously optimised by 7.38%, 8.93%, 5.69% and 12.64% respectively, compared to traditional 1:1 situation. Therefore, the concentration ratio is an important factor for further improvement of thermocell performance.

The dependences of performance on concentration revealed in this paper provide basic guidance for future concentration

optimisation and the electrode potentials measured are essential data for numerical modelling of thermocell. Additionally, it should be noted that this research is based on a U-tube thermocell which has a significant distance between electrodes. For the future study of scenarios with a short distance between electrodes, Soret effect, the polarization of the electrode and convection need to be investigated in order to determine how they influence the performance of thermocell.

Acknowledgements

The support from the Newton Fund under UK-China Joint Research and Innovation Partnership Fund (Grant number 201703780098), the Royal Academy of Engineering through the Transforming Systems through Partnerships program (Grant number TSP1098) and grants from the National Natural Science Foundation of China (Grant numbers No. 51976176 and No. 51806189), the Fundamental Research Funds for the Central Universities (Grant number 2020QNA4008),China Science Foundation (Grant numbers 2018M640556 and 2019T120514) and from Zhejiang Province Science Foundation under grant number ZJ20180099 are gratefully acknowledged. The authors also would like to recognise the support from NSFC-RS Joint Project (Grant numbers No. 5151101443 and IE/151256).

References

[1] H. Ali, B.S. Yilbas, A. Al-Sharafi. Innovative design of a thermoelectric generator with extended and segmented pin configurations. Applied Energy. 187 (2017) 367-79.

[2] S. Shittu, G. Li, X. Zhao, X. Ma, Y.G. Akhlaghi, E. Ayodele. High performance and thermal stress analysis of a segmented annular thermoelectric generator. Energy Conversion and Management. 184 (2019) 180-93.

[3] B. Li, K. Huang, Y. Yan, Y. Li, S. Twaha, J. Zhu. Heat transfer enhancement of a modularised thermoelectric power generator for passenger vehicles. Applied Energy. 205 (2017) 868-79.

[4] F.N. Al-Mousawi, R. Al-Dadah, S. Mahmoud. Low grade heat driven adsorption system for cooling and power generation using advanced adsorbent materials. Energy Conversion and Management. 126 (2016) 373-84.

[5] Y. Lu, A.P. Roskilly, K. Tang, Y. Wang, L. Jiang, Y. Yuan, et al. Investigation and performance study of a dual-source chemisorption power generation cycle using scroll expander. Applied Energy. 204 (2017) 979-93.

[6] A. Godefroy, M. Perier-Muzet, N. Mazet. Thermodynamic analyses on hybrid sorption cycles for low-grade heat storage and cogeneration of power and refrigeration. Applied Energy. 255 (2019) 113751.

[7] F. Alshammari, A. Pesyridis. Experimental study of organic Rankine cycle system and expander performance for heavy-duty diesel engine. Energy Conversion and Management. 199 (2019) 111998.

[8] Z. Li, X. Yu, L. Wang, Y. Lu, R. Huang, J. Chang, et al. Effects of fluctuating thermal sources on a shell-and-tube latent thermal energy storage during charging process. Energy. 199 (2020) 117400.

[9] Y. Lu, A.P. Roskilly, X. Yu, K. Tang, L. Jiang, A. Smallbone, et al. Parametric study for small scale engine coolant and exhaust heat recovery system using different Organic Rankine cycle layouts. Applied Thermal Engineering. 127 (2017) 1252-66.
[10] C.-G. Han, X. Qian, Q. Li, B. Deng, Y. Zhu, Z. Han, et al. Giant thermopower of ionic gelatin near room temperature. Science. (2020) eaaz5045.
[11] R. Chen, S. Deng, W. Xu, L. Zhao. A graphic analysis method of electrochemical systems for low-grade heat harvesting from a perspective of thermodynamic cycles. Energy. 191 (2020) 116547.
[12] J. Hu, S. Xu, X. Wu, D. Wu, D. Jin, P. wang, et al. Multi-stage reverse electrodialysis: Strategies to harvest salinity gradient energy. Energy Conversion and Management. 183 (2019) 803-15.
[13] Z. Fang, L. Jia, W. Yang, B.E. Logan. A thermally regenerative ammonia-based battery for efficient harvesting of low-grade thermal energy as electrical power. Energy & Environmental Science. 8 (2014) 343-9.
[14] F. Giacalone, F. Vassallo, L. Griffin, M.C. Ferrari, G. Micale, F. Scargiali, et al. Thermolytic reverse electrodialysis heat engine: model development, integration and performance analysis. Energy Conversion and Management. 189 (2019) 1-13.
[15] Y. Wang, L. Cai, W. Peng, Y. Zhou, J. Chen. Maximal continuous power output and parametric optimum design of an electrochemical system driven by low-grade heat. Energy Conversion and Management. 138 (2017) 156-61.
[16] X. Wang, Y.-T. Huang, C. Liu, K. Mu, K.H. Li, S. Wang, et al. Direct thermal charging cell for converting low-grade heat to electricity. Nature Communications. 10 (2019) 4151.
[17] K. Kim, S. Hwang, H. Lee. Unravelling ionic speciation and hydration structure of Fe(III/II) redox couples for thermoelectrochemical cells. Electrochimica Acta. 335 (2020) 135651.
[18] T. Shibata, H. Iwaizumi, Y. Fukuzumi, Y. Moritomo. Energy harvesting thermocell with use of phase transition. Scientific Reports. 10 (2020) 1813.
[19] T. Li, X. Zhang, S.D. Lacey, R. Mi, X. Zhao, F. Jiang, et al. Cellulose ionic conductors with high differential thermal voltage for low-grade heat harvesting. Nature Materials. 18 (2019) 608-13.
[20] X. Zhu, M. Rahimi, C.A. Gorski, B. Logan. A Thermally-Regenerative Ammonia-Based Flow Battery for Electrical Energy Recovery from Waste Heat. Chemsuschem. 9 (2016) 873-9.
[21] W. Wang, G. Shu, H. Tian, D. Huo, X. Zhu. A bimetallic thermally-regenerative ammonia-based flow battery for low-grade waste heat recovery. Journal of Power Sources. 424 (2019) 184-92.
[22] S.W. Lee, Y. Yang, H.W. Lee, H. Ghasemi, D. Kraemer, G. Chen, et al. An electrochemical system for efficiently harvesting low-grade heat energy. Nature Communications. 5 (2014) 3942.
[23] G. Qian, Y. Lu, Y. Huang, Z. Li, X. Yu, A.P. Roskilly. Simulation study of Ferricyanide/Ferrocyanide concentric annulus thermocell with different electrode spacing and cell direction. Energy Procedia. 142C (2017) 374-80.
[24] M.F. Dupont, D.R. Macfarlane, J.M. Pringle. Thermo-electrochemical cells for waste heat harvesting - progress and perspectives. Chemical Communications. 53 (2017).
[25] H. Im, H.G. Moon, J.S. Lee, Y.C. In, T.J. Kang, Y.H. Kim. Flexible thermocells for utilization of body heat. Nano Research. 7 (2014) 443-52.
[26] P. Yang, K. Liu, Q. Chen, X. Mo, Y. Zhou, S. Li, et al. Wearable Thermocells Based on Gel Electrolytes for the Utilization of Body Heat. Angew Chem Int Ed Engl. 55 (2016) 12050-3.
[27] J. Duan, B. Yu, K. Liu, J. Li, P. Yang, W. Xie, et al. P-N conversion in thermogalvanic cells induced by thermo-sensitive nanogels for body heat harvesting. Nano Energy. 57 (2019) 473-9.
[28] A. Gunawan, N.W. Fette, P.E. Phelan. Thermogalvanic Waste Heat Recovery System in Automobiles. ASME 2015 Power Conference Collocated with the ASME 2015 International Conference on Energy Sustainability, the ASME 2015 International Conference on Fuel Cell Science, Engineering and Technology, and the ASME 2015 Nuclear Forum2015. p. V001T11A2.
[29] R. Hu, B.A. Cola, N. Haram, J.N. Barisci, S. Lee, S. Stoughton, et al. Harvesting waste thermal energy using a carbon-nanotube-based thermo-electrochemical cell. Nano Letters. 10 (2010) 838-46.
[30] A.H. Kazim, A.S. Booeshaghi, S.T. Stephens, B.A. Cola. Thermo-electrochemical Generator: Energy Harvesting & Thermoregulation for Liquid Cooling Applications. Sustainable Energy & Fuels. (2017).
[31] T.I. Quickenden, Y. Mua. A Review of Power Generation in Aqueous Thermogalvanic Cells. Journal of The Electrochemical Society. 142 (1995) 3985-94.

[32] Y. Mua, T.I. Quickenden. Power conversion efficiency, electrode separation, and overpotential in the ferricyanide/ferrocyanide thermogalvanic cell. Journal of the Electrochemical Society. 143 (1996) 2558-63.
[33] L. Zhang, T. Kim, N. Li, T.J. Kang, J. Chen, J.M. Pringle, et al. High Power Density Electrochemical Thermocells for Inexpensively Harvesting Low-Grade Thermal Energy. Advanced Materials. 29 (2017) 1605652-n/a.
[34] H. Im, T. Kim, H. Song, J. Choi, J.S. Park, R. Ovalle-Robles, et al. High-efficiency electrochemical thermal energy harvester using carbon nanotube aerogel sheet electrodes. Nature Communications. 7 (2016).
[35] A. Gunawan, C.-H. Lin, D.A. Buttry, V. Mujica, R.A. Taylor, R.S. Prasher, et al. Liquid Thermoelectrics: Review of Recent And Limited New Data of Thermogalvanic Cell Experiments. Nanoscale & Microscale Thermophysical Engineering. 17 (2013) 304-23.
[36] T.J. Kang, S. Fang, M.E. Kozlov, C.S. Haines, L. Na, H.K. Yong, et al. Electrical Power From Nanotube and Graphene Electrochemical Thermal Energy Harvesters. Advanced Functional Materials. 22 (2012) 477–89.
[37] N.E. Holubowitch, J. Landon, C.A. Lippert, J.D. Craddock, M.C. Weisenberger, K. Liu. Spray-Coated Multiwalled Carbon Nanotube Composite Electrodes for Thermal Energy Scavenging Electrochemical Cells. ACS Applied Materials & Interfaces. 8 (2016) 22159-67.
[38] M.A. Buckingham, F. Marken, L. Aldous. The thermoelectrochemistry of the aqueous iron(ii)/iron(iii) redox couple: significance of the anion and pH in thermogalvanic thermal-to-electrical energy conversion. Sustainable Energy & Fuels. (2018).
[39] J.H. Kim, J.H. Lee, R.R. Palem, M.-S. Suh, H.H. Lee, T.J. Kang. Iron (II/III) perchlorate electrolytes for electrochemically harvesting low-grade thermal energy. Scientific Reports. 9 (2019) 8706.
[40] M. Al Maimani, J.J. Black, L. Aldous. Achieving pseudo-'n-type p-type' in-series and parallel liquid thermoelectrics using all-iron thermoelectrochemical cells with opposite Seebeck coefficients. Electrochemistry Communications. 72 (2016) 181-5.
[41] T.J. Abraham, D.R. Macfarlane, R.H. Baughman, L. Jin, N. Li, J.M. Pringle. Towards ionic liquid-based thermoelectrochemical cells for the harvesting of thermal energy. Electrochimica Acta. 113 (2013) 87-93.
[42] M.A. Lazar, D. Almasri, D.R. Macfarlane, J.M. Pringle. Enhanced thermal energy harvesting performance of a cobalt redox couple in ionic liquid-solvent mixtures. Physical Chemistry Chemical Physics Pccp. 18 (2016) 1404.
[43] T.J. Abraham, D.R. Macfarlane, J.M. Pringle. High Seebeck coefficient redox ionic liquid electrolytes for thermal energy harvesting. Energy & Environmental Science. 6 (2013) 2639-45.
[44] T. Kim, J.S. Lee, G. Lee, H. Yoon, J. Yoon, T.J. Kang, et al. High thermopower of ferri/ferrocyanide redox couple in organic-water solutions. Nano Energy. 31 (2017) 160-7.
[45] M. Bonetti, S. Nakamae, M. Roger, P. Guenoun. Huge Seebeck coefficients in nonaqueous electrolytes. The Journal of Chemical Physics. 134 (2011) 114513.
[46] J. Duan, G. Feng, B. Yu, J. Li, M. Chen, P. Yang, et al. Aqueous thermogalvanic cells with a high Seebeck coefficient for low-grade heat harvest. Nature Communications. 9 (2018) 5146.
[47] M.S. Romano, S. Gambhir, J.M. Razal, A. Gestos, G.G. Wallace, J. Chen. Novel carbon materials for thermal energy harvesting. Journal of Thermal Analysis and Calorimetry. 109 (2012) 1229-35.
[48] A.J. Bard, L.R. Faulkner. Electrochemical Methods Fundamentals and Applications. 2nd ed. John Wiley & Sons, Inc., New York, 2001.
[49] H. Zhou, T. Yamada, N. Kimizuka. Supramolecular Thermo-Electrochemical Cells: Enhanced Thermoelectric Performance by Host–Guest Complexation and Salt-Induced Crystallization. Journal of the American Chemical Society. 138 (2016) 10502-7.
[50] T. Yamada, X. Zou, Y. Liang, N. Kimizuka. A supramolecular thermocell consisting of ferrocenecarboxylate and beta-cyclodextrin that has a negative Seebeck coefficient. Polymer Journal. 50 (2018) 771-4.
[51] W.M. Haynes, D.R. Lide, T.J. Bruno. CRC Handbook of Chemistry and Physics: A Ready-Reference Book of Chemical and Physical Data. 95th ed. CRC Press, Boca Raton, FL, USA, 2014.
[52] S.R. DeGroot, P. Mazur. Non-Equilibrium Thermodynamics. Dover Publications, New York, 2011.
[53] H. Saraç, M.A. Patrick, A.A. Wragg. Physical properties of the ternary electrolyte potassium ferri-ferrocyanide in aqueous sodium hydroxide solution in the range 10–90°C. Journal of Applied Electrochemistry. 23 (1993) 51-5.